July 2003

Leaders in Cutting Edge Technology

Software, Hardware and Services for The Engineering Community

LEAP Australia	**Altair Western Region US**	**DYNAMAX US**	**Cril Technology Simulation France**
GISSETA India	**MFAC Canada**	**DYNA*more* Germany**	**Flotrend Taiwan**
KOSTECH Korea	**ERAB Sweden**	**THEME Korea**	**ALTAIR Italy**
CAD-FEM Germany	**Numerica SRL Italy**	**ANSYS China**	
Dr. Ted. Belytschko US	**Dr. Bhavin V. Mehta US**	**Dr. Taylan Altan US**	**Dr. David Benson US**
Dr. Alexey L. Borovkov Russia	**Prof. Gennaro Monacelli Italy**	**Prof. Ala Tabiei US**	

Articles

Editor	Trent Eggleston
Editor – Technical Content	Arthur B. Shapiro
Technical Writer	Dr. David Benson
Technical Writer	Uli Franz
Graphic Designer	Sandy Boling
Graphic Designer	Wayne Mindle
Feature Director	Marsha J. Victory

Large Data Visualization for Everyone

SGI brings Advanced Visualization to Departmental Computing with NEW SGI ONYX 350 and Visual Area Networking Capabilities.

reprinted from http://www.sgi.com/features/2003/apr/onyx350/index.html

Since its introduction a year ago, Visual Area Networking (VAN) has broken down barriers between end users, collaborative teams, and the large data sets that bring competitive advantage to their organizations. With more than 100 installations in the government and defense, science, manufacturing, energy industries, VAN is accelerating data access and product design cycles around the world. SGI recently enhanced these capabilities with new VAN software and the new SGI Onyx 350 system at an entry price of $33,390 USLP--the lowest ever for an SGI® Onyx® system--to extend those benefits to departments large and small.

The Large Data Visualization Challenge

The new combined solution addresses an escalating problem: Ever-increasing data sets create a growing bottleneck for distributed organizations and collaborative work environments. The time it takes to copy models from computer centers to analysis workstations and to enable collaboration by replicating large models and simulation results to several systems can quickly erode much of the potential productivity benefits of high-resolution analysis and distributed collaboration.

Network and system limitations also make effective large data analysis and collaboration difficult, even over a departmental LAN. Most workstations can't interact with data of 5GB or more, so users are forced to view data piecemeal or in low resolution, thus stealing time and sapping productivity from every project. Organizations today demand a solution that doesn't require them to retool or invest in massive network upgrades--and yet still empowers them to accelerate workflows in distributed and collaborative environments.

Better Decisions Faster

Fortunately, SGI has the solution. By implementing VAN environments with the new SGI Onyx 350 system, departments empower users to break through the traditional organizational walls that hinder true collaborative computing, while affordably overcoming the limitations of desktop systems. This new solution allows single users and workgroups to make better decisions faster by leveraging a true supercomputer architecture with parallel CPUs, massive shared memory, and scalable I/O bandwidth to handle a department's big data sets. This powerful system enables all data to be visualized at once--a capability that UNIX® and Windows® OS-based workstations simply cannot match. As a result, design cycles can be shortened by up to 20%.

This combined solution gives an entire department access to supercomputing power coupled with advanced visualization--whether engineers are local or collaborating with others around the globe. Now multiple users can share control of a single interactive, visual application--without having to copy multi-gigabyte data sets between sites and without the need for additional graphics technology on remote user workstations.

Networked Visualization and Collaboration for a Large Data World

When deployed on a VAN, the new SGI Onyx 350 system acts as a visual server to augment an organization's desktop systems. Each system supports up to eight independent remote users or collaborative sessions, with each session including up to five different networked collaborators who see and share control of a single virtual environment. The compact, cost-effective nature of this new solution allows organizations to double the number of local, remote, or collaborative visualization sessions that can be supported within a fixed departmental budget.

The new OpenGL Vizserver™ 3.1 software is a key component for implementing VAN environments and enables application-transparent, multiuser collaboration. Using OpenGL Vizserver, the application and data reside on the server where all 3D rendering takes place using full hardware acceleration. Rendered images then are compressed and delivered to the client workstation. Since this eliminates data copying, VAN puts instant,

interactive access to a visualization supercomputer on every desk in a department. By leveraging this breakthrough, any individual or distributed group can interact with a large data set, no matter what their desktop limitations may be.

Now multiple users can share control of a single interactive, visual application–without having to copy multi-gigabyte data sets between sites and without the need for additional graphics technology on remote user workstations.

New features within OpenGL Vizserver software include multiuser collaboration, stereo visualization for remote and collaborative sessions on SGI® clients, support across firewalls, and support for the Windows® XP Tablet PC operating system to enable a common environment for mobile computing users. SGI Visual Area Networking supports clients running SGI® IRIX®, Sun™ Solaris™, Linux®, and Microsoft® Windows®.

Advanced Visualization for Any Department

Two advanced visualization solutions are available to meet the demanding needs of engineers and scientific researchers. Both solutions are based on the new Onyx 350 system and offer up to 32 600 MHz or 700 MHz MIPS® R16000™ processors, 64GB of high-performance shared memory, and maximum I/O rates of over 22GB per second via multiple independent PCI-X buses. These solutions also add new digital media capabilities and deliver dramatic new levels of price/performance in a compact form factor that makes high-productivity visualization and collaboration available to any department.

SGI Onyx 350 InfinitePerformance™: Stocked with faster I/O buses and modules--along with twice the available memory of previous models--this new system brings supercomputer-based advanced visualization to the lowest price ever. Starting at $33,390 USLP and packed with all of the features and performance of Onyx and InfinitePerformance graphics, this new system brings all the benefits of advanced visualization to even small departments. In addition, Onyx 350 can scale to up to eight independent InfinitePerformance graphics pipelines that can be used independently or can be combined with optional Scalable Graphics Compositors to deliver higher levels of visual performance.

SGI Onyx 350 InfiniteReality4™: This compact, midrange scalable visualization system supports up to eight InfiniteReality4 graphics pipelines and increases compute power, memory size, I/O speed and digital media capabilities. Each InfiniteReality4 pipeline offers 1GB of texture memory so complex models can run quickly, 8 subsample anti-

aliasing for the highest image quality, and eight output channels with over 8 million pixels of display so photo-realistic images can be used by individuals or teams.

Optimized Large Data Visualization Solutions

By combining the new SGI Onyx 350 system and VAN capabilities, users can maximize departmental and distributed resources across all technical and creative computing marketplace segments, including:

- Manufacturing: A new SGI Onyx 350 system with InfinitePerformance allows engineers to tackle complex designs and analyze sophisticated problems that would be impossible on desktop UNIX or Windows systems, while new VAN capabilities allow them to accomplish this independent of their locations. This allows engineering design cycles to be reduced by as much as 20%.

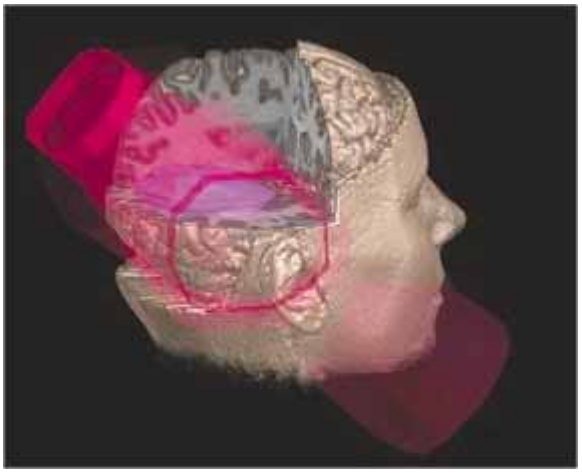

- Education and research: SGI VAN and Onyx 350 solutions bring advanced visualization power to the grid. For the first time, grid users and collaborative teams are able to immediately visualize and understand supercomputer results, no matter the size of those results or where they are located. New multiuser collaboration and stereo capabilities in OpenGL Vizserver 3.1 allow distributed teams to interactively manipulate and visualize a single model in an immersive environment. This can accelerate a research program by up to 100 times.

- Energy exploration and production: The most advanced well drilling and reservoir analysis techniques often involve 50GB to 500GB of data. Only SGI Onyx systems combine the I/O bandwidth, memory size, and unrivaled 3D volume visualization capabilities needed to analyze large data sets required for well drilling and reservoir management. The new SGI Onyx 350 system allows up to 64GB of memory, improving price/performance by as much as 35%

- Command and control: Today's homeland security and national defense environments rely heavily on having an accurate and up-to-date common operating picture for decision makers at headquarters and in the field. Only the Onyx 350

system with InfinitePerformance combines the power of supercomputing with the insights of advanced visualization and the distributed collaboration of VAN. These solutions are compact and require less power, making them suitable for deployment at forward command centers or with mobile units.

- Film processing and mastering: Requiring maximum I/O bandwidth and compute power, high-quality film processing and mastering demand truly integrated visualization to maintain quality control. The size, power, and digital media capabilities of SGI Onyx 350 systems increase rack density by 400% and deliver a greater than 30% decrease in total cost of ownership.

EIGENVALUE COMPARISONS

With the release of version 960 LS-DYNA has a powerful eigenvalue analysis capability built on the start-of-the-art Block Shifted and Inverted Lanczos package BCSLIB-EXT from Boeing. With version 970 we have included the necessary modeling capabilities so that an eigenvalue analysis in LS-DYNA will match those from NASTRAN. To do this we have included new linear shell elements and additional constraint capabilities for the NASTRAN RBE2 and RBE3 constraints.

NASTRAN input file

- Component with approximately 60,000 equations
- Spotwelds use brick elements with RBE3 constraints
  - 2022 RBE3's (*CONSTRAINED_INTERPOLATION)
  - 12 RBE2's (*CONSTRAINED_NODAL_RIGID_BODY)
- Eigenvalue solution for free-free modes
  - 6 rigid body modes
- Solved eigenvalue problem with types 18 and 20 linear elements and types 6 and 16 nonlinear elements
  - Shell elements types 18 and 20 were within 2% of NASTRAN, CQUAD4, eigenvalues—some slightly smaller others larger, but generally larger.

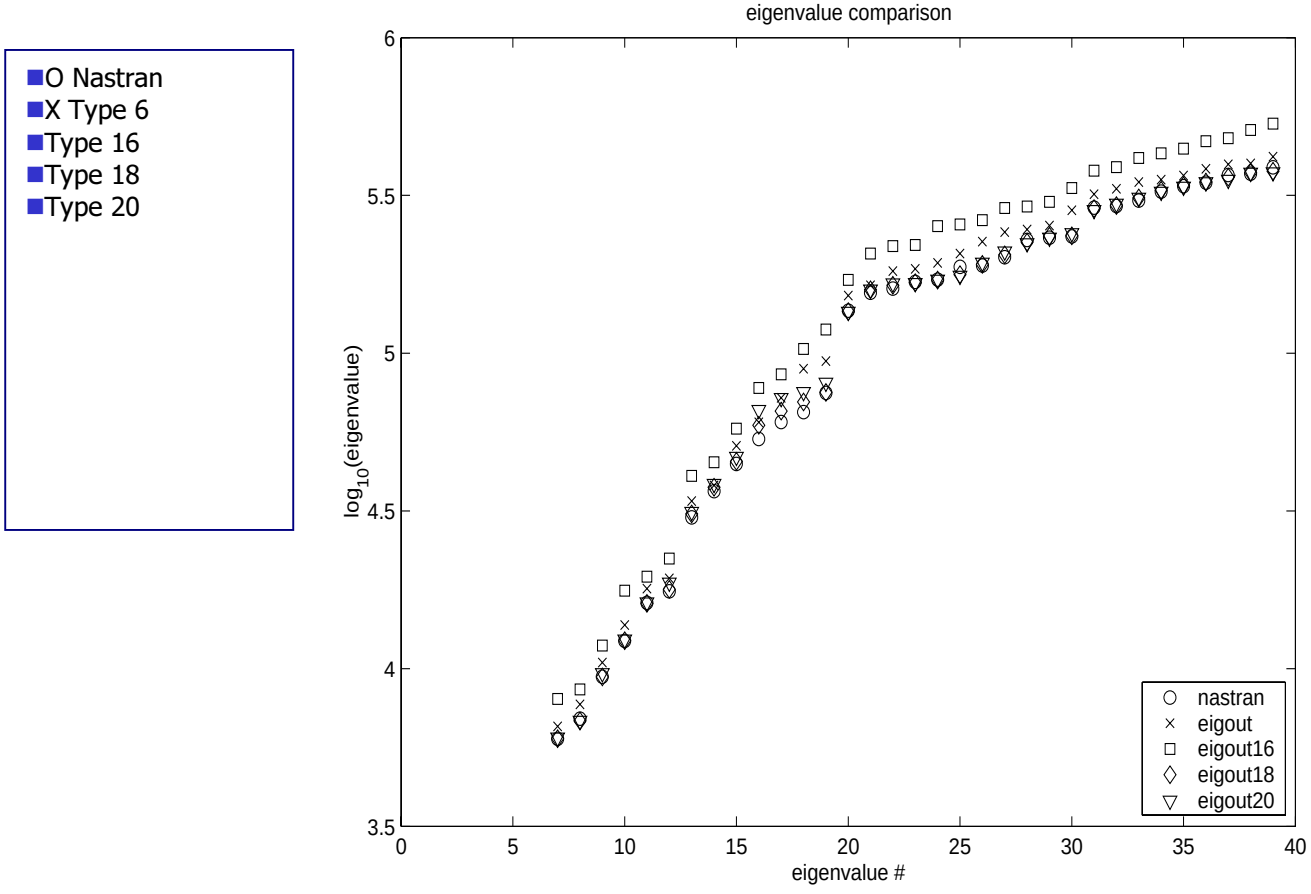

Eigenvalue Extraction

We have also added an exciting new eigenvalue analysis capability in version 970. At any time during the simulation, whether implicit or explicit, the simulation can be interrupted and an eigenvalue analysis performed. The simulation then resumes from the interrupted state. Users can now determine the normal modes of their models at various stages during the simulation. And this analysis can be performed seamlessly with their simulation.

- **Frequencies and Mode Shapes Change During Simulation**
  - tensile stress increases natural frequency (guitar string)
  - contact with obstacles changes mode shapes

- **LS-DYNA Can Extract Eigenvalues During Transient Analysis**
  - curve gives time to extract eigenvalues, how many to extract
  - implicit or explicit transient analysis
  - new database family for each set of eigenvalues

- **Simple Input Parameters**
  - *CONTROL_IMPLICIT_GENERAL
    - nIMFLAG = 1: implicit with intermittent eigenvalues
    - nIMFLAG = 6: explicit with intermittent eigenvalues
  - *CONTROL_IMPLICIT_EIGENVALUE
    - NEIGV = -(curve ID) on

FEA Information Participants
Commercial and Educational

Headquarters	Company	
Australia	Leading Engineering Analysis Providers	www.leapaust.com.au
Canada	Metal Forming Analysis Corp.	www.mfac.com
China	ANSYS – China	www.ansys.com.cn
France	Cril Technology Simulation	www.criltechnology.com
Germany	DYNA*more*	www.dynamore.de
Germany	CAD-FEM	www.cadfem.de
India	GissEta	www.gisseta.com
Italy	Altair Engineering srl	www.altairtorino.it
Italy	Numerica srl	www.numerica-srl.it
Japan	The Japan Research Institute, Ltd	www.jri.co.jp
Japan	Fujitsu Ltd.	www.fujitsu.com
Japan	NEC	www.nec.com
Korea	THEME Engineering	www.lsdyna.co.kr
Korea	Korean Simulation Technologies	www.kostech.co.kr
Russia	State Unitary Enterprise - STRELA	www.ls-dynarussia.com
Sweden	Engineering Research AB	www.erab.se
Taiwan	Flotrend Corporation	www.flotrend.com
UK	OASYS, Ltd	www.arup.com/dyna
USA	INTEL	www.intel.com
USA	Livermore Software Technology	www.lstc.com
USA	Engineering Technology Associates	www.eta.com
USA	ANSYS, Inc	www.ansys.com
USA	Hewlett Packard	www.hp.com
USA	SGI	www.sgi.com
USA	MSC.Software	www.mscsoftware.com
USA	DYNAMAX	www.dynamax-inc.com
USA	AMD	www.amd.com
Educational Participants		
USA	Dr. T. Belytschko	Northwestern University
USA	Dr. D. Benson	Univ. California – San Diego
USA	Dr. Bhavin V. Mehta	Ohio University
USA	Dr. Taylan Altan	The Ohio State U – ERC/NSM
USA	Prof. Ala Tabiei	University of Cincinnati
Russia	Dr. Alexey I. Borovkov	St. Petersburg State Tech. University
Italy	Prof. Gennaro Monacelli	Prode – Elasis & Univ. of Napoli, Federico II

Special Announcements and Highlights of News Pages

Posted on FEA Information and archived one month on the News Page

June 02	**ANSYS**	ANSYS WorkBench Environement
	LSTC	LS-PrePost – LS-OPT
	DYNA*more*	Germany: Distributor
June 09	**ACTA**	Sent new AVI for our library
	MSC Software	NASTRAN
	JRI	JMAG
	Altair – Italy	Italy: Distributor
June 17	**SGI**	Visual Networking
	ETA	FEMB
June 24	**OAYSIS**	Primer
	HP	Workstation zx6000
	CADFEM	Germany: Distributor
June 30	**Xiandong Xue**	Sent new AVI's for our library
	INTEL	Intel® Pentium® 4 processor
	FUJITSU	Primepower
	LEAP	Australia: Distributor

Events & Courses from the Events page on www.feainformation.com

Oct 02-05	**Int' Conference on CAE**	**Italy**
Oct 14-15	**The Japan Research Institute LS-DYNA & JMAG Users Conference**	**Japan**
Oct 29-31	**Testing Expo North America**	**USA**
Nov 11	**LS-DYNA Update Forum from DYNAmore (free of charge)**	**Germany**
Nov 12 –14	**CAD-FEM User Conference**	**Germany**
Nov 18-19	**MSC. Software Virtual Product Development Conf.**	**UK**
2004 May 2-4	**8th International LS-DYNA Users conference will again be held at the Hyatt Regency Dearborn, Fairlane Town Center, Dearborn, MI hosted by LSTC and ETA**	**US**

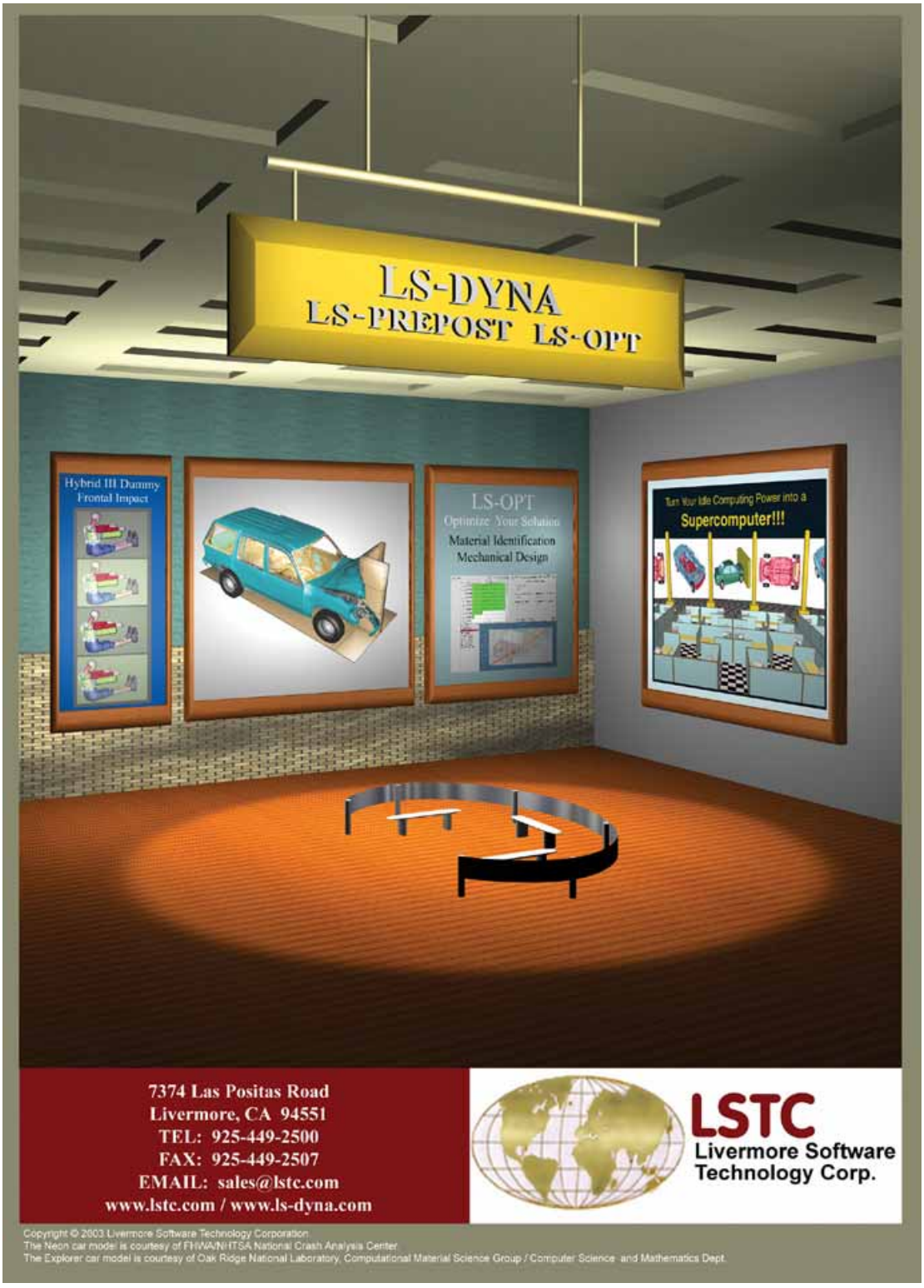

LS-DYNA: a general-purpose transient dynamic finite element program capable of simulating complex real world problems. LS-DYNA comes with LS-PREPOST and LS-OPT at no additional charge:

LS-PrePost: Model editor and post-processor

LS-OPT: A tightly integrated optimization code.

AN INVESTIGATION OF THE APPARENT MASS OF PARACHUTES UNDER POST INFLATION DYNAMIC LOADING THROUGH THE USE OF FLUID STRUCTURE INTERACTION SIMULATIONS

A. P. Taylor
Irvin Aerospace Inc
Santa Ana, California

Abstract

This paper presents the application of a commercially available Fluid Structure Interaction (FSI) simulation tool post inflation problems in parachute systems. Steady state performance and post inflation dynamic loading are explored for an arbitrary cross parachute design.

Additionally, the affect of mesh boundary location on these results is explored.

Introduction

The understanding of post inflation dynamic loading of parachutes continues to be the realm of expensive testing rather than analysis and simulation. This is not only costly in terms of program dollars, but also can be costly to system performance.

Post inflation loading can include events such as vehicle reorientation for landing position orientation or load retraction for soft landing. In both areas, the parachute apparent mass and canopy skirt deformation are significant contributions that simple spring mass type simulations find difficult to fully represent.

In the reorientation case, we know from experience that these events can have loads equal to or higher than to original parachute inflation loads. We also know that common simulation techniques (spring/mass/drag simulations) tend to over predict these loads by 10% or higher. Structural efficiency and, in some cases, customer confidence, is lost due to poor predictions.

For the retractor cases, a level of performance is lost to the same phenomena, and the landing sweet spot can be significantly changed by the combination of structural elongation, skirt deformation and dumping of the entrapped air mass.

This paper will explore the aspects of post inflation dynamic loading through the use of Fluid Structure Interaction simulations. Along the way, as a matter of model development and checkout, we will also review variations in modeling technique, such as boundary location and parachute performance, such as the variation of drag coefficient with canopy loading (W/S).

Approach

The Explicit Finite Element Analysis (FEA) tool LS-DYNA will be employed for this investigation. Irvin has used this tool for many years for the analysis of fabric structures, including airbags, impact nets, and highly technical static fabric structures.

The LS-DYNA tool currently includes two fluid solvers with further extension ongoing. The most mature of these solvers is a Navier-Stokes solution based on the Arbitrary LaGrange-Eulerian (ALE) solution method. In this approach, the fluid mesh computation includes a LaGrangian phase, where the fluid mesh is allowed to move. This can greatly reduce the cost (computational overhead) associated with solution of the Navier-Stokes (NS) equations. At intervals, either every computational frame or user selected, the fluid mesh is moved back to its original (or Eulerian) position. During this process, fluid mass must be conserved and, in the case of multi-material fluids, individual element characteristics must be updated. This process is often referred to as “advection”. For all simulations in this paper, advection was completed at every time step (integration step). While reduction of the advection frequency can greatly improve computational overhead, the models presented herein have acceptable performance and the limited number of similar runs did not require run time optimization.

Fluid/structural coupling is completed within the LS-DYNA solver. This approach provides significant flexibility to the user as fluid and structural meshes can be totally independent. A simple series of input cards dictate coupling between various parts – in this case, the fluid and the parachute structure. In other applications, this might be cords in an automotive tire or re-bar in a concrete structure.

During the solution, the LS-DYNA solver completes coupling through penalty method, between the fluid and the parachute structure. This approach eliminates significant problems such as fluid mesh distortion.

It is one of our purposes with this article to begin to establish validation of this technique in our application area, specifically, fluids and fabric structures.

For this effort, a full symmetry model of a cross parachute was initially created. However, the majority of simulations were completed using a quarter symmetry model for computational overhead.

The cross geometry is somewhat arbitrary and is discussed below; model size will be varied to isolate the effects of mass and drag. The model is initiated with the parachute in a flat "as built" configuration and fluid flow "inflates" the parachute to a flying shape.

The parachute structure includes suspension lines and structural elements that represent radials and skirt bands. Figure 1 presents views of the basic structural mesh. Shell elements representing the parachute drag surface use the LS-DYNA *mat_fabric material model which eliminates bending stiffness and has little to no compressive stiffness. Similarly, beam elements used have no compressive stiffness. For simplicity, linear moduli are used in the tensile regime. However, fully non-linear characteristics, including hysteretic behavior, are available for both the shell and beam elements.

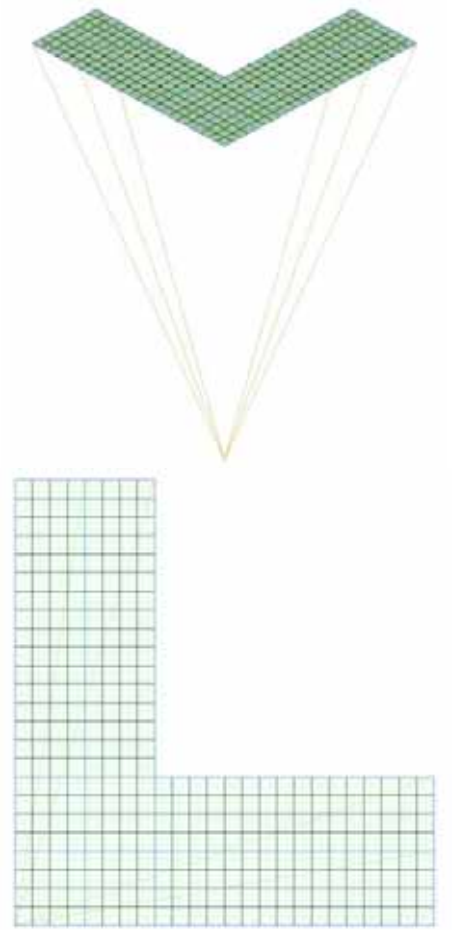

Figure 1. Basic Model – Parachute Structural Mesh

Figure 2 presents a view of the initial fluid mesh with the constructed parachute shape.

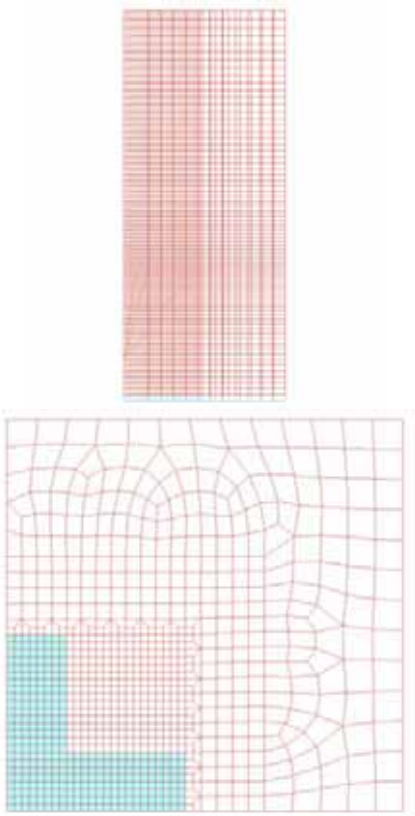

Figure 2. Basic Model – Parachute and Fluid Mesh

Model Checkout

Several steps were taken to validate the cross parachute model and simulation results prior to the analysis of post inflation dynamics. These analyses include the evaluation of boundary location and the variation of the parachute drag coefficient with flight velocity or canopy loading (w/s). The latter is a well-understood trend in most parachutes and the demonstration of a representative trend is pursued to provide some confidence in the FSI results.

Parachute Loading (w/s) Validation

One of the most common parachute performance parameters, and perhaps the simplest to validate in an FSI simulation, is the relationship between canopy loading (or rate of descent) and the drag performance, as measured by drag coefficient, of the parachute. The higher the canopy loading, or descent flight condition, the lower the drag coefficient. This effect is presented in Reference 1 and many others.

Our current simulation technique is an infinite mass flight, that is, the parachute lines are constrained and the air passes by the parachute, much as would happen in a vertical wind tunnel. Therefore, in this simulation environment, the weight loading is reflected as an increasing velocity in the fluid passing by the retained parachute. Velocity variations from 18.0 to 36.0 fps were selected.

One of the first conclusions we reached was that the parachute drag should be evaluated at the same non-dimensional inflation time for all simulations. As we know, parachutes inflate as a function of the true airspeed at which they are inflating. Therefore, for these relatively short inflation simulations (1-2 seconds), evaluation at the same "quasi-stable" point was important. That is to say, that since these results were taken approximately 0.5 to 1.0 seconds after initial inflation, the parachute drag results are still relatively un-damped.

As a result, all results presented in this section are based on a similar inflation velocity time. For instance, the 18.0 fps inflation results are taken at 2.0 seconds in the simulation. Similarly, the 36.0 fps results are taken at 1.0 second in the simulations. All other results are a ratio of the fluid (inflation) velocity, and the 36.0 fps/1.0 second result.

Our original result is presented in Figure 3. The plot provides a variation of parachute drag coefficient versus "free stream" dynamic pressure.

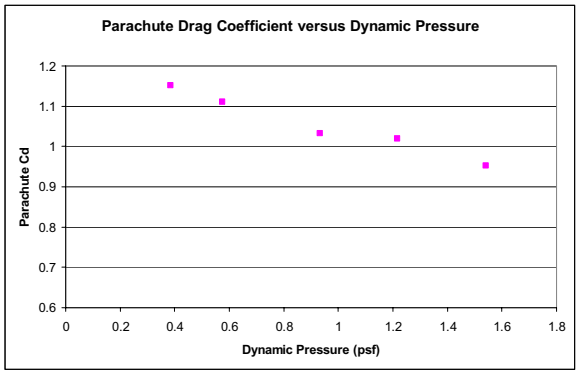

Figure 3. Parachute Drag Coefficient (Cd) versus Flight Dynamic Pressure

While the trend in the drag coefficient is similar to measured data (Ref 1) and encouraging, the mean value of the drag coefficient seams questionable. First, the overall value is too high. Two potential explanations occur for this. The first is that the parachute model, while being a cross configuration, is constructed of zero permeability fabric – permeability models are currently being developed. Furthermore, the boundary conditions for quarter symmetry result in a zero permeability parachute with perfect stability. Therefore, we would expect the Drag Coefficient (Cd) for this simulation to be rather high. Parachute drag coefficient is based on constructed (planform) area of the cross parachute.

However, the resulting Cd is high enough that we decided to review the boundary conditions and related blockage effects for this model.

Boundary Location Variation and Computational Cost

As discussed above, the rather high Cd results initiated a review of the mesh boundary location. One metric that we will use for this evaluation is the ratio of parachute constructed or planform area to the vertical cross section of the fluid mesh. We were surprised to discover that this was approximately 11% for the original model but this model was basically created on "looks good criteria". Additionally, this ratio is the ratio of constructed parachute area and flow area and is not directly related to classic wind tunnel blockage area. A true blockage might be closer to 4-6%.

At this point, two additional fluid meshes were completed by extending the outer elements in both the vertical cross section (flow area) and the entrance and exit locations for the fluids. Figure 4 presents a comparison of the original and two new, extended fluid mesh models.

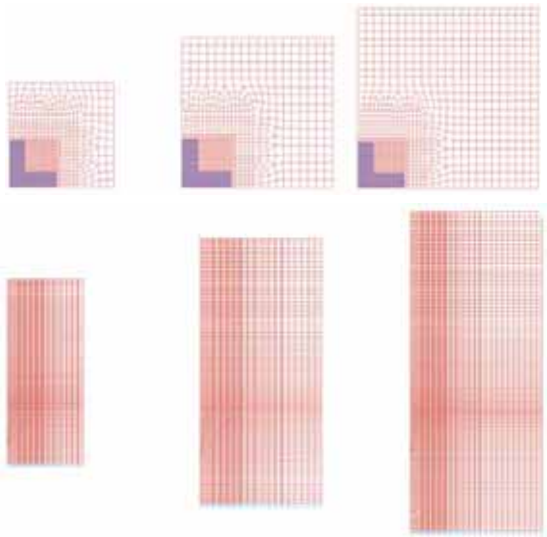

Figure 4. Comparison of Original and Extended Boundary Models

The 28.0 fps model was used as the comparison point between these three fluid mesh models. All runs were completed to the same time period and drag data were reduced to coefficient form in the same manner.

Figure 5 provides a plot of parachute drag coefficient versus the planform to flow area ratio. The 11.25% entry is the original model. While not yet asymptotic, the 4-6% ratio area begins to look acceptable for engineering solutions. That is to say, we are not looking for absolute engineering data from these class of simulations, but rather accurate comparisons between configurations variations. Thus, we believe that some level of absolute accuracy can be sacrificed in exchange for improved computation overhead (run time).

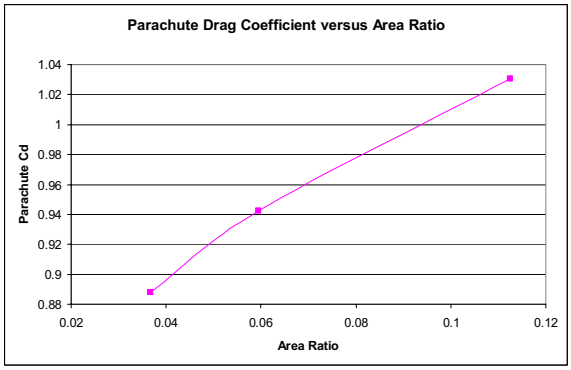

Figure 5. Drag Coefficient Results versus Area Ratio – Original and Extended Boundaries

The lack of expected asymptotic behavior is likely related to the fact the extended boundary models increase the fluid flow area and move the inlet and exit flow boundaries further from the structural elements. Figure 6 provides a comparison of parachute Cd with total element count for the models. Here we see an expected asymptotic behavior on Cd with increasing element count.

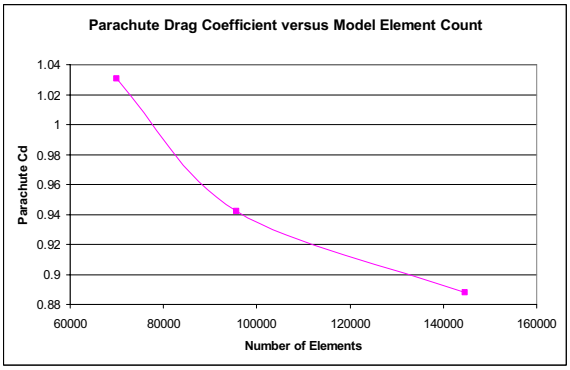

Figure 6. Drag Coefficient versus Element Count – Extended Boundary Models

Figure 7 provides plot of computational cost (run time hours) versus the resulting parachute drag coefficient. We see that a significant additional cost is paid for the relatively small overall accuracy increase from 6% to 4% of the ratio.

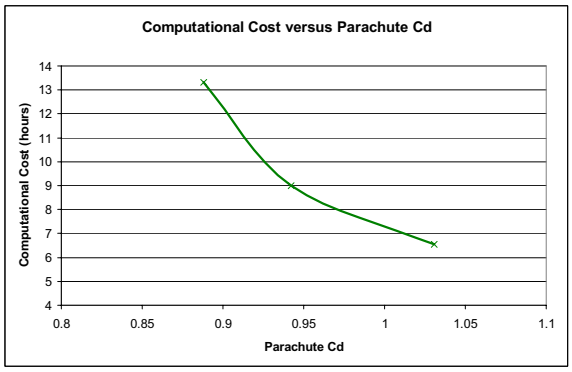

Figure 7. Computational Cost versus Drag Coefficient Result

We therefore conclude that the 6% model represents the appropriate balance between run time and accuracy, at least for this exercise.

Finally, Figure 8 presents the relationship between computational cost (run time) and number of elements for these three models.

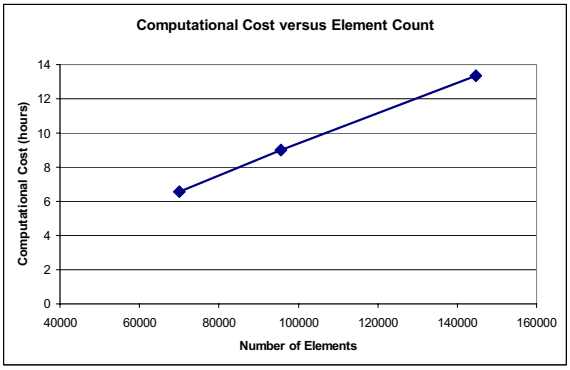

Figure 8. Computation Cost versus Element Count

Updated Parachute Loading Validation

A new w/s run series was completed using the middle or 6% ratio model. The same flight velocities were used with the fluid mesh being the only change. Figure 9 presents the Cd versus dynamic pressure variation from this series of runs. The curve again has the expected slope. We are not aware of any significant database for cross parachutes, particularly of any specific arm length ratio. However, our purpose is only to demonstrate that the variation can be analyzed with these tools.

As the Cd variation (versus canopy loading or flight speed) is known to be related to canopy shape, our next logical step would be to review the simulation results of shape differences. Figure 9 provides a comparison between the 18.0 and 36.0 fps simulations. For

emphasis, we also completed a similar simulation for a 60 fps flight condition. This helps to further illustrate the change in canopy shape with canopy loading or increased flight speed. Note the flattening of the parachute crown, reduced extension of the parachute arm, and tightening radius in the shoulder region, all with increasing airspeed.

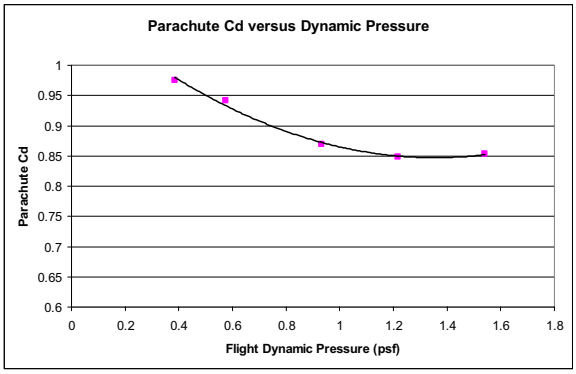

Figure 9. Final Result – Parachute Drag Coefficient versus Flight Dynamic Pressure

Figure 10. Parachute Shape Comparison – Various Flight Airspeeds

Retraction Models

The stated goal of this paper is to investigate the post inflation dynamics of parachutes. That is, how fully inflated canopies respond to load variations. For Irvin, the most interesting of these events is the reorientation of a vehicle, such as a UAV. This typically occurs following main parachute inflation and is done to adjust the vehicle from the initial parachute deployment condition to one more favorable for landing.

Our experience is that if not carefully controlled, these events can produce loads as high or higher than those experienced during initial parachute inflation. In the simplest model, this process involves the release of the parachute(s), and the subsequent retraction or re-loading of the parachutes by the cargo.

For the purposes of this paper, we will consider only the retraction phase. This will eliminate the computational cost (time) related to the release, as well as an independent variable, the time or distance that the parachute is released. Additionally, this approach will provide some insight, if not a simulation baseline, prior to investigating the more complicated maneuver.

Our approach therefore, is to complete several simulations of a retraction of the same parachute and fluid mesh. The basic difference between simulations will be the linear size of the parachute and fluid mesh. Retraction events will be scaled to provide the same average velocity during the retraction phase. Additionally, as the linear stroke is scaled with the mesh size, the parachute will traverse the same portion of the fluid mesh.

As the parachute drag should scale with the square of the linear dimension (call it lambda) and the trapped fluid mass scales with the cube of lambda, we hope to isolate or at least provide insight into the relation between drag and inertial forces during these types of events.

Figure 10 provides an example of an FSI simulation of a cross parachute during a retraction event.

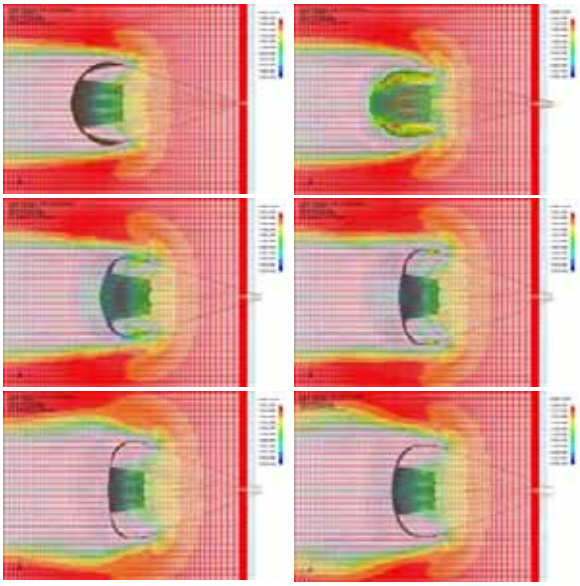

Figure 10. Cross Parachute under Retraction Load

Scaled Retraction Velocity

Following several developmental simulations, an initial series of runs were completed. In these, we used the scaled fluid and structural meshes, but the same material definitions throughout. Our simulations included, 1, 3, 7 and 10 times scale factor.

A preliminary review indicated that the structural differences between the models, while not severe, were definitely influencing results.

Figure 11 presents a comparison of the 1 and 10 times scale simulations at the same point during retraction. Both the additional suspension line extension and the skirt collapse related deformation (also related to the suspension lines) were enough to convince us that this approach would not provide technical fidelity. The approach was initially adopted due to concern about computational overhead and, to some extent, an attempt to eliminate another scaling factor, that being structural strength.

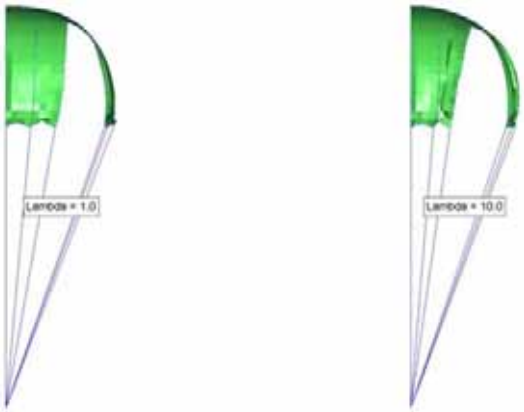

Figure 11. Shape Comparison During Retraction – Different Parachute Size, Same Fabric Strengths

Scaled Retraction Velocity and Scaled Structure

Following the conclusion that parachute structure would require scaling with the linear dimension (lambda), those enhancements were made to the model. Shell elements representing the broadloom areas of the parachute were scaled by increasing the shell thickness linearly with the lambda parameter. This approach provides additional fabric weight along with strength and, therefore, the overall simulation run time is not impacted. Additionally, this is a reasonable reflection of the overall situation. In reality, the smallest parachute configurations are probably at a minimum weight (or gauge) condition, resulting in the larger models being heavier than required, however, this approach provides an excellent means for apples-to-apples comparison.

The linear structure, suspension lines, radials and horizontal reinforcements were scaled with the square of the linear dimension (lambda). Simulation results have shown that these adjustments do not significantly impact simulation cost, at least in the context of these models.

Table 1 provides a summary of the models completed and the input conditions for these simulations. Unfortunately, these results were completed in parallel with the boundary location analysis presented above. They are, therefore, for the smallest or original fluid model. The next section will present similar results for the extended boundary model.

Table 1. Input Conditions for Scaled Retraction Models

Lambda	*Flight Velocity*	*Stroke*	*Retraction Time*	*Retract Velocity*
1	28 fps	5.6 inches	.0133 sec.	421.1 in/sec
3	28 fps	16.8 inches	.0399 sec.	421.1 in/sec
7	28 fps	39.2 inches	.0931 sec.	421.1 in/sec
10	28 fps	56.0 inches	.1330 sec.	421.1 in/sec

Figure 13 provides a summary of the force data for all four models. These plots were completed by summing the Z-axis force component for each of the suspension line elements (one per line) and multiplying by four to represent the entire canopy. Actually, one of the two center arm elements was dropped to not over account for this line, which is, theoretically, split by the two symmetry planes.

Since the force term is computed from the suspension lines, it represents a combination of drag and inertial related terms during the retraction event.

The shape of the force versus time curves in Figure 13 suggest a drag dominated reaction for lambda = 1. For lambda = 7 and 10, the peak force is clearly inertial related.

Figure 14 provides a summary of the peak retraction force versus the canopy size parameter lambda.

In Figure 15, we add a simple rigid body drag calculation during retraction and a least squares regression type fit to the simulation results and the simple drag calculation. The second quadratic curve on the plot represents the drag force for a rigid body of equal drag coefficient to the steady, pre-retraction parachute CdS, assuming that this body is at the flight velocity of the descending parachute, plus the retraction velocity. We can see that the peak force is well above the drag only predicted force.

The drag calculation is a true quadratic equation based on the variation of drag area with the square of lambda. Thus, even when a cubic fit was selected, the cubic term is returned as zero.

The similar coefficient on the squared or area related term and the dominant cubic or volume related term in

the simulation results curve fit suggests that inertial terms related to the parachute volume are truly dominant. This is, of course, a fact that we knew and expected, but we are excited about the implications for model validation that these results suggest.

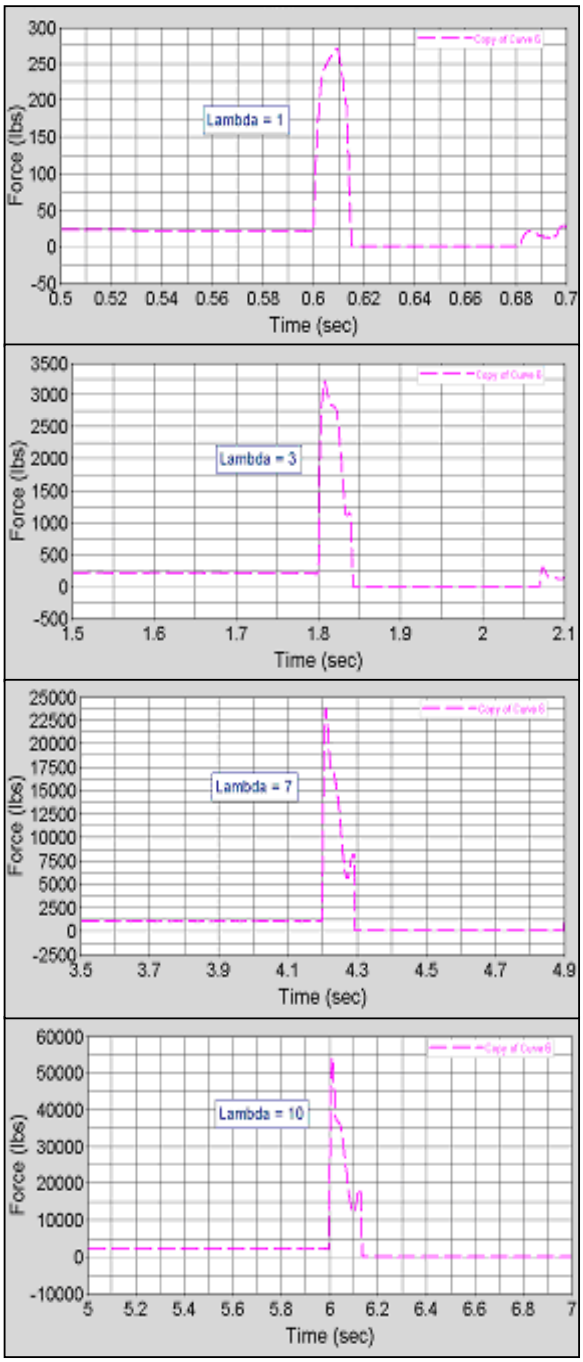

Figure 13. Force Time History during Retraction Event

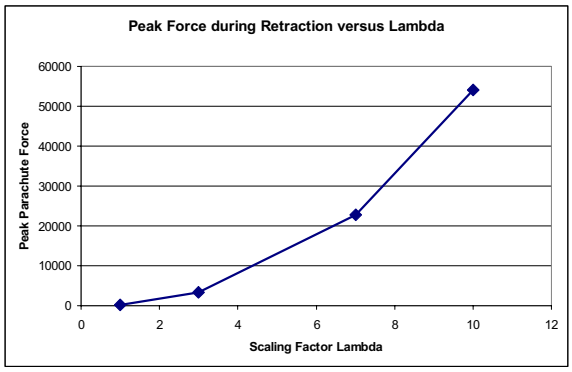

Figure 14. Peak Retraction Force versus Scaling Factor

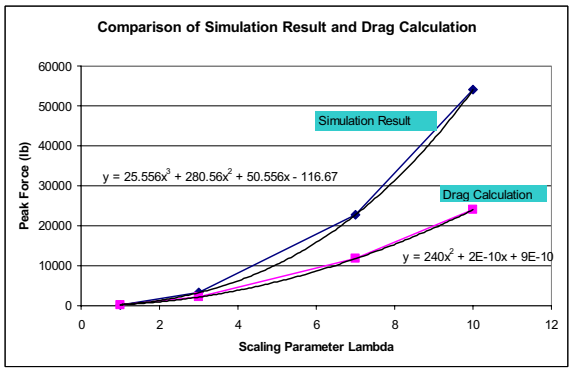

Figure 15. Curve Fits of Peak Retraction Force and Rigid Body Drag for Retraction Velocity

Next, we complete a simple spring, mass, drag area model for the retraction scenarios. The parachute drag area is set to the steady parachute drag area from the results above. Suspension lines are represented by an equivalent spring of the same length and stiffness. Parachute mass is computed, for first order, as a sphere having the radius of the inflated parachute (0.67 of overall arm length) and using the FSI simulation air density. This is a simplification of the classic computations for apparent/included mass is taken, as none of this work is directly related to post inflation dynamic loading. Additionally, we expect none would be directly related to the arbitrary cross parachute in this report.

In each case, the suspension line confluence is retracted in an infinite mass method. Parachute velocity is the super position of steady state flight (28.0 fps) and the added velocity from the retraction event. These computations were completed using a simple spreadsheet approach.

Figure 16 provides a comparison between the FSI results and the simple spreadsheet model discussed above. We find a reassuringly similar trend between the peak force in the spring/mass/drag model and the full

FSI model. Again this suggests a level of validation for the FSI solution.

In Figure 17, we arbitrarily adjust the volume that is used to compute the parachute apparent/included mass. This adjustment is made once, and the resulting volume is scaled across the range of the lambda scale factor. With this approach we see a relatively good correlation between FSI and the simple spreadsheet computation. Again, this suggests to us a level of validation for the FSI tool.

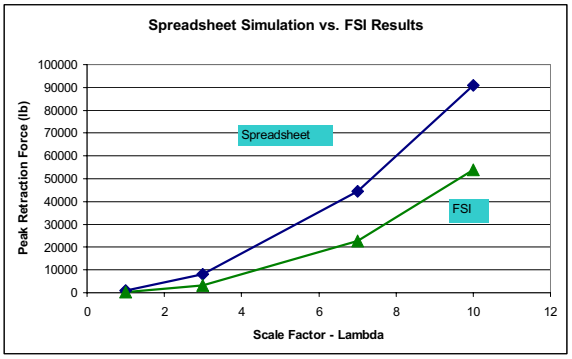

Figure 16. Peak Force Comparison – FSI Results and Spreadsheet Simulation

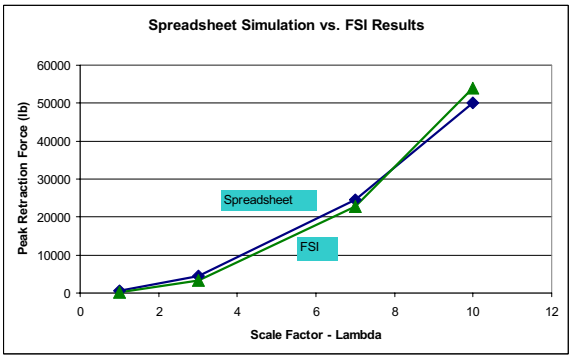

Figure 17. Peak Force Comparison – FSI Results and Spreadsheet Simulation – Parachute Included Mass Adjusted

Scaled Velocity and Structure with Extended Boundary

The original retraction models were completed prior to full understanding of the boundary location data presented above. Fortunately, sufficient time remains to repeat the retraction runs with the extended boundary (middle size) mesh, as presented above.

Figure 18 presents a comparison between the original results and the extended boundary model; clearly, the mesh boundary locations are not as significant for the retraction event. This result also indicates that the previous comparisons remain valid.

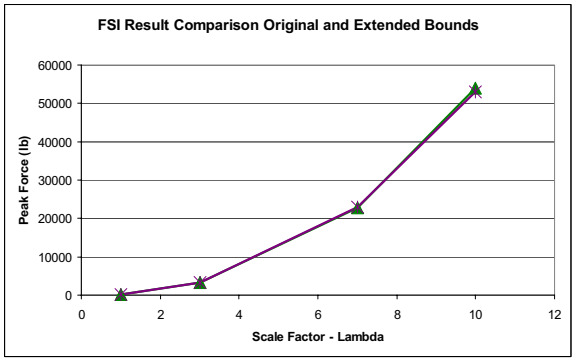

Figure 18. FSI Retraction Results (Original and Extended Boundary)

Future Investigations

The results presented throughout this paper concentrated on a cross parachute of generic design. This is primarily because this is one of the simplest parachutes to draw.

The application of these tools is certainly not limited to cross type parachutes. Previously, we have had difficulty with solution of flat, circular parachutes. This may be related to inter-gore contact and a resulting fluid/structure coupling issue. However, it is most likely the result of an early, incorrect model.

Most recently, we have explored the application of FSI to shaped, round parachutes. These are much more applicable to the world of high performance recovery systems. Figure 19 provides an interim result from a FSI solution for a solid, quarter-spherical construction parachute. We expect and are hopeful that this model will exhibit unstable flight due to vortex shedding and the resultant fluid structure interactions.

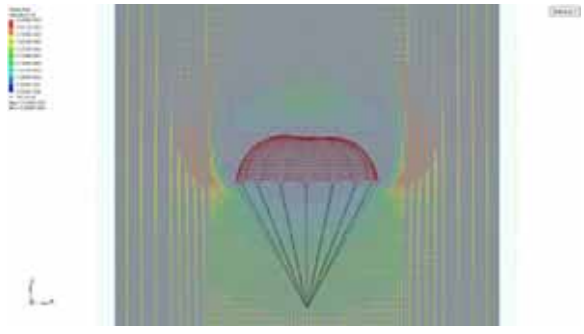

Figure 19. Interim Result, Full Symmetry Simulation of Round Parachute – Wake Re-contact Event

With the demonstration of this basic result (an unstable parachute), we can then begin to modify the parachute configuration to enhance stability.

The overall relationship between parachute stability and drag coefficient as established through FSI can provide a significant enhancement to recovery system performance.

Similarly, Figure 20 provides an early result for a 3-cell model of a parafoil portion. Our purpose here was to demonstrate the ability to model these devices, including the internal flow aspects of parafoils. The unique plot provides an opaque contour of the fluid velocity field and a view of the structural deformations of fabric structure.

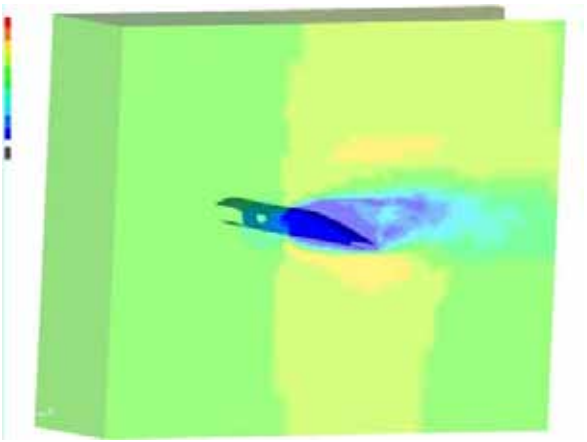

Figure 20. FSI Result – Parafoil Section

Eventually, we believe is will be possible to use FSI computations for a variety of performance predictions for these devices. These might include projection of airfoil shape in flight, optimization of line set geometry variations in anhedral geometry, and performance enhancements such as local rigidization.

Other features of the FSI code are being exercised as well. For instance, the LS-DYNA tool provides a feature for mesh following which allows a free falling parachute simulation. The problem is simplified by specifying a fluid mesh that follows the falling parachute, thus significantly reducing the problem size. We are currently working to complete boundary condition definitions and then will begin simple validation simulations like those presented herein.

The unique coupling algorithm in LS-DYNA allows significant cross flow, or shear type motion of the structure. This is much more difficult for algorithms that directly couple the fluid and structural mesh and the fluid elements are quickly distorted. As a result, we are beginning to use this FSI approach for de-spin analysis of payloads such as spinning missiles.

Additionally, we continue to cooperate with software vendors for algorithm and tool enhancement. LSTC will shortly add a porosity algorithm to the ALE coupling, allowing the simulation of parachute fabrics with real world permeability.

Altair Engineering has recently added significant post-processing features to their products to support the analysis and data reduction of these simulations.

Conclusions

We find these results to be somewhat compelling. However, it must be recognized that these very early simulations are rather simple when compared to the world of modern recovery systems. These models lack many of the sophisticated details of today's high performance designs, such as slots, gaps and sails.

Additionally, our validation results are anecdotal at best, lacking the rigorous details of flight to simulation comparisons or even a program specific/flight proven parachute design.

However, it was our simple objective to demonstrate the emerging use of FSI tools, including commercially available solvers, to perform the beginnings of true parachute performance analysis in a virtual (or simulation) environment.

The solutions presented were all completed on a modern but commercial PC class workstation. Average solution times were 6-14 hours. In general, models were meshed, completed, and post-processed on a modern PC class laptop computer.

We are convinced that these tools are on the near horizon for our industry and will offer a significant leap in recovery system understanding and performance – perhaps as significant as the introduction of Kevlar was in the 1970's.

In summary, the future is bright – the computer is coming to the recovery system industry.

References

1. P. Delurgio. Evolution of the Ringsail Parachute. AIAA 99-1700. June 1999.